OPEN

NPG Asia Materials (2017) 9, e343; doi:10.1038/am.2016.203
www.nature.com/am

ORIGINAL ARTICLE

Resonant level-induced high thermoelectric response in indium-doped GeTe

Lihua Wu[1], Xin Li[1,2], Shanyu Wang[3], Tiansong Zhang[4], Jiong Yang[1], Wenqing Zhang[1], Lidong Chen[4] and Jihui Yang[3]

Resonant levels are promising for high-performance single-phase thermoelectric materials. Recently, phase-change materials have attracted much attention for energy conversion applications. As the energetic position of resonant levels could be temperature dependent, searching for dopants in phase-change materials, which can introduce resonant levels in both low and high temperature phases, remains challenging. In this study, possible distortions of the electronic density of states due to group IIIA elements (Ga, In, Tl) in GeTe are theoretically investigated. Resonant levels induced by indium dopants in both rhombohedral and cubic phase GeTe have been demonstrated. The experimental Seebeck coefficients of $In_xGe_{1-x}Te$ exhibit a large enhancement compared with those observed for other prior dopants. Indium dopants reduce the defect concentrations in GeTe, and thus, they lower the carrier concentrations and suppress the electronic component of the total thermal conductivity. The enhanced Seebeck coefficient, together with the suppressed thermal conductivity, leads to a reasonably high ZT of 1.3 at a temperature near 355 °C in $In_{0.02}Ge_{0.98}Te$. The corresponding average ZT is enhanced by ~70% across the entire temperature range of the rhombohedral and cubic phases. These observations indicate that indium-doped GeTe is a promising base material for achieving an even higher thermoelectric performance.

NPG Asia Materials (2017) **9,** e343; doi:10.1038/am.2016.203; published online 20 January 2017

INTRODUCTION

Thermoelectric materials can directly convert thermal gradients to electricity, and vice versa. The performance of thermoelectric materials can be described by the figure of merit ZT, $ZT = S^2T/\rho\kappa$. Herein, S, T, ρ, and κ denote the Seebeck coefficient, absolute temperature, electrical resistivity, and total thermal conductivity (including the lattice and electronic components), respectively.[1–3] The lattice thermal conductivity κ_L can typically be reduced via a low sound velocity,[4] a large lattice anharmonicity,[5–8] rattling atoms in lattice voids,[9–11] or even liquid-like sublattices,[12–15] and multi-scale microstructures.[16–20] The electronic properties can be improved by band convergence,[21–26] dimensionality reduction,[1,27–29] and resonant levels.[2,30] By modulating the electronic and thermal terms, the figure of merit and energy conversion efficiency of thermoelectric materials can be optimized for widespread applications.

GeTe is a narrow band gap IV–VI compound,[31] which exhibits rhombohedral and cubic crystal structures in low and high temperatures, respectively, due to a ferroelectric phase transition at ~370 °C.[32] Due to high concentrations of Ge vacancies,[33] GeTe shows *p*-type conduction behavior in both phases. The common strategies for the optimization of GeTe are reducing the hole concentrations and the thermal conductivity.[34] Over the years, GeTe-based materials have been regarded as high-performance thermoelectric materials and components, especially GeTe-$AgSbTe_2$ solid solutions (known as TAGS).[35] In TAGS, a figure of merit ZT >1.5 can be achieved by controlling the Ag/Te ratio[36] or doping rare earth Ce, Yb and Dy.[37,38] Recently, Pb dopants in GeTe were successfully used to optimize the carrier concentration and form sub-micron phase separation domains to reduce the thermal conductivity, which resulted in a ZT of ~2 for $Pb_xGe_{1-x}Te$.[39] Bi_2Te_3-doped $Pb_xGe_{1-x}Te$ has also been reported with an excellent ZT of ~1.9.[40] $Sb_xGe_{1-x}Te$ compounds showed a similar ZT of ~1.85 and high mechanical stability.[41] Therefore, GeTe can provide a versatile lead-free base material for thermoelectric applications.[34]

However, the influence of resonant levels on the thermoelectric response of GeTe warrants further exploration. Resonant levels can be introduced through interactions between the dopants and the host. The dopants normally have similar electronic configurations as the host atoms, and they are usually selected from the neighboring main group elements,[42] such as doping Tl on the Pb-site of PbTe,[2,30] Sn on the Bi-site of Bi_2Te_3,[43] Pb on the Bi-site of BiCuSeO,[44] and In on the Sn-site of SnTe.[45] The modified density of states (DOS) obtained by

[1]Materials Genome Institute, Shanghai University, Shanghai, China; [2]Department of Physics, College of Sciences, Shanghai University, Shanghai, China; [3]Department of Materials Science and Engineering, University of Washington, Seattle, WA, USA and [4]State Key Laboratory of High Performance Ceramics and Superfine Microstructure, Shanghai Institute of Ceramics, Chinese Academy of Sciences, Shanghai, China
Correspondence: Professor Jiong Yang or Professor W Zhang, Materials Genome Institute, Shanghai University, 99 Shangda Road, E-433, Shanghai 200444, China.
E-mail: jiongy@t.shu.edu.cn or wqzhang@t.shu.edu.cn
or Professor Jihui Yang, Materials Science and Engineering Department, University of Washington, 315 Roberts Hall, Box 352120, Seattle, WA 98195, USA.
E-mail: jihuiy@uw.edu
Received 1 September 2016; revised 25 October 2016; accepted 16 November 2016

the resonant levels can have an important effect on the Seebeck coefficients of thermoelectric materials. The Mott relationship shows the fundamental expression of the Seebeck coefficient:[46]

$$S = \frac{\pi^2 k_B^2 T}{3q} \cdot \frac{\mathrm{d}[\ln(\sigma(E))]}{\mathrm{d}E}\bigg|_{E=E_F} = \frac{\pi^2 k_B^2 T}{3q} \cdot \left[\frac{1}{p(E)}\frac{\mathrm{d}p(E)}{\mathrm{d}E} + \frac{1}{\mu(E)}\frac{\mathrm{d}\mu(E)}{\mathrm{d}E}\right]\bigg|_{E=E_F}. \quad (1)$$

Herein, k_B and $\sigma(E)$ are the Boltzmann constant and the energy-dependent electrical conductivity. Equation (1) indicates that the energy dependence of the carrier concentration p or mobility μ near the Fermi level determines the Seebeck coefficient. Critical scattering near phase transitions and charge-carrier relaxation can lead to an abrupt change of $\mu(E)$.[47,48] However, a large $\mathrm{d}p(E)/\mathrm{d}E$ could also originate from an unconventional distortion of the DOS by the introduction of proper dopants, as aforementioned, which is another fundamental reason for the enhanced Seebeck coefficients.

Recently, phase-change materials have attracted significant attention for high-performance energy conversion.[8,12,49] Searching for dopants in a phase-change material, which can induce resonant levels in both the low- and high-temperature phases, would be technically useful for thermoelectric applications. The energetic positions of resonant levels could be temperature dependent in IV–VI compounds due to the relative energy shifts of the host states and resonant levels when the temperature changes.[2] The shifted Fermi level can also hinder the beneficial effect of resonant levels on the electrical properties. In this study, *ab initio* calculations and experiments are carried out to study the possible resonant levels in GeTe by doping the materials with group IIIA elements. Among them, indium dopants in GeTe are found to create strong resonant levels in both the rhombohedral and the cubic phases. In our experiments, In-doped GeTe compounds exhibit significantly enhanced Seebeck coefficients. The reduced hole concentration as the In content increases indicates that the dopants help to reduce the intrinsic Ge vacancies. The increased electrical resistivity, due to the lowering of the carrier concentration and mobility, reduces the total thermal conductivity and leads to a relatively high ZT of 1.3 near 355 °C in the $In_{0.02}Ge_{0.98}Te$ compound. The average ZT is enhanced by ~70% across the entire temperature range. The resonant levels induced by indium doping make $In_xGe_{1-x}Te$ attractive for further optimization.

EXPERIMENTAL PROCEDURES

Theoretical calculations

The DOS was obtained by first-principles calculations with the Vienna *ab initio* simulation package (VASP).[50] Generalized gradient approximation[51] and projected augmented wave methods[52,53] were adopted in the calculations. We adopted a $4\times4\times4$ supercell of the formula unit GeTe for all the calculations in the rhombohedral and cubic phases, including the ones with vacancies or group IIIA dopants. Vacancies in $Ge_{63}Te_{64}$ were found to have no effect on the total DOS. All crystal structures were fully relaxed before the DOS calculations. The theoretical transport properties (the carrier concentration dependence of the Seebeck coefficient) were calculated by combining density functional theory (DFT) with the Boltzmann transport formula, based on the constant relaxation time approximation.[54,55] The spin-orbit coupling effect can have a strong influence on the band structure and DOS of GeTe,[56] which was considered in all the first-principles calculations.

Synthesis of $In_xGe_{1-x}Te$ samples

The $In_xGe_{1-x}Te$ ($x=0$, 0.01, 0.02, 0.03, 0.04, 0.05, 0.06) compounds were synthesized by melting stoichiometric elements In, Ge, and Te (99.999%, Sigma-Aldrich, St Louis, MO, USA) in sealed quartz tubes. The mixtures were first kept at 1050 °C for 24 h, subsequently slowly cooled to ~500 °C and held for 70 h. The grown ingots were ground into fine powders in agate mortars. Powders were sintered into bulk materials in a spark plasma sintering (SPS) System using a graphite die with a diameter of 12.7 mm under a pressure of 45 MPa. The crystal structure is determined by X-ray diffraction (XRD) on a Rigaku D/max 2200 (Rigaku Corporation, Tokyo, Japan). The XRD patterns are shown in Supplementary Figure S1. The phase purity and compositions are examined using a Zeiss Supra 55 scanning electron microscope (SEM) with an Oxford energy dispersive spectrometer (EDS). SEM and EDS elemental mapping results are presented in Supplementary Figures S2–S4.

Measurements of thermoelectric properties

The Seebeck coefficient (S) and electrical resistivity (ρ) for $In_xGe_{1-x}Te$ from room temperature to ~460 °C were measured on an ULVAC ZEM-3 system using bar samples (~$2.5\times2.5\times8$ mm^3) cut from the sintered pellets. The total thermal conductivity of $In_xGe_{1-x}Te$ was determined from the thermal diffusivity (α), density (D) and heat capacity (C_p) using the equation $\kappa = C_p \times D \times \alpha$, where the thermal diffusivity (α) was measured by a Netzsch LFA 457. Archimedes' method was used to determine the densities of the sintered samples, while the heat capacity was estimated by the Dulong-Petit law. The differences in the rhombohedral and cubic phases were considered. The uncertainties of the measured electric resistivity, Seebeck coefficient, and calculated thermal conductivity were estimated at approximately 5, 5, and 10%, respectively.

Hall effect measurements

Hall measurements were performed on thin bar samples (~$2\times7\times0.6$ mm^3) in a physical property measurement system (PPMS) equipped with a 9-T magnet (up to ±3T used in this work) to determine the room temperature carrier concentration and mobility. The Hall measurements were verified by comparing the results with those obtained from ^{125}Te NMR methods.[34] The Hall coefficients (R_H) of $In_xGe_{1-x}Te$ were calculated from the slopes of Hall voltage vs magnetic field curves. Then, the carrier concentration (p) and Hall mobility (μ) were calculated from the Hall coefficients and electrical resistivity using the relations, $p=\beta/|eR_H|$ and $\mu=|R_H|/\rho$, respectively, where β is approximately equal to unity for degenerate GeTe compounds.

RESULTS AND DISCUSSION

Possible distortions of the DOS due to group IIIA elements (Ga, In, Tl) in GeTe were first determined by *ab initio* calculations. Figure 1a shows the DOS of GeTe ($Ge_{64}Te_{64}$) and $In_{0.016}Ge_{0.984}Te$ ($InGe_{63}Te_{64}$) in their room temperature rhombohedral phases. For stoichiometric GeTe, the Fermi level is located in the middle of the band gap. However, due to large amounts of intrinsic Ge vacancies, binary GeTe compounds in the experiments usually have high hole concentrations. The Fermi level falls deeply into the valence band (VB), which leads to the p-type transport behavior of GeTe. When the indium dopants are introduced, the total DOS is distorted near the VB maximum (VBM). The *ab initio* calculations for $In_{0.016}Ge_{0.984}Te$ exhibit two states induced by the In: the hyper-deep states at −5 ~ −6 eV below the VBM (not shown here) and the deep defect states (DDSs) right above the VBM, which pin the Fermi level (Figure 1a). The DDS is caused by the hybridization between In and the host, with $5p^1$ from In instead of $5s^2$. As shown in Figure 1a, 20% of the DDS are composed of In, 10% from Ge, 50% from Te, and the rest are interstitial states. The DDS is originally a fully filled bulk band in GeTe, and it is pulled upwards and becomes half-filled due to the In dopant, which implies that each In supplies one hole when it substitutes Ge in GeTe (forming the defect $In_{Ge}^{'}$). At high temperatures, GeTe transforms into a face-centered cubic structure. The transition temperature is ~370 °C, depending on the alloying contents. By considering the working temperature range of GeTe-based thermoelectric materials, which is across the phase transition point, the mechanism by which In-doping alters the DOS of the cubic phase is another important question. Figure 1b shows GeTe and the In-doped compound in their face-centered cubic phases.

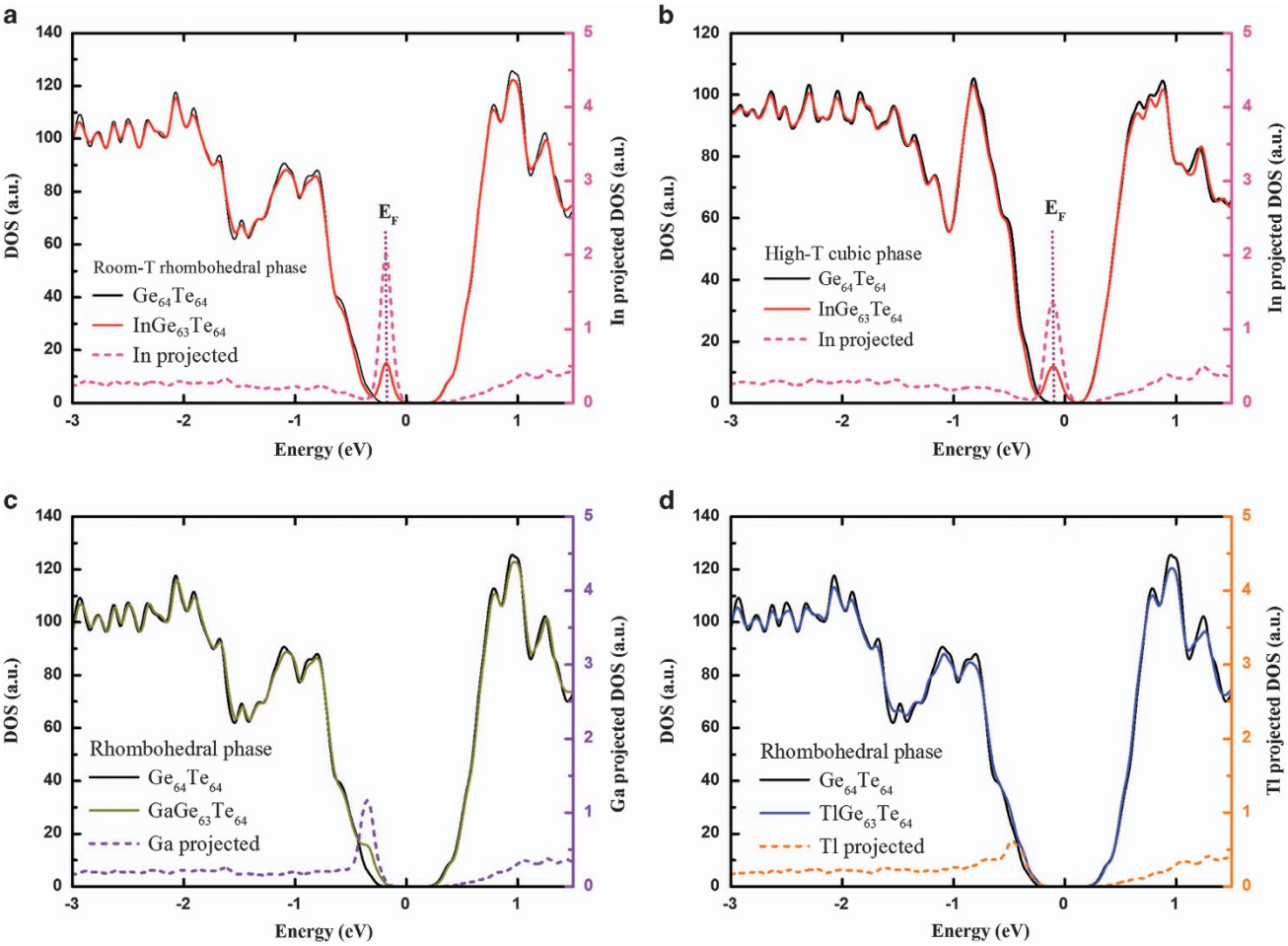

Figure 1 The calculated density of states (DOS) for (**a**) room temperature rhombohedral phase GeTe ($Ge_{64}Te_{64}$) and $In_{0.016}Ge_{0.984}Te$ ($InGe_{63}Te_{64}$); (**b**) high-temperature cubic phase $Ge_{64}Te_{64}$ and $InGe_{63}Te_{64}$; (**c**) rhombohedral $GaGe_{63}Te_{64}$; and (**d**) rhombohedral $TlGe_{63}Te_{64}$. The In, Ga, and Tl projected DOS and the Fermi levels in $InGe_{63}Te_{64}$ are included. $InGe_{63}Te_{64}$ shows an abrupt change of DOS at E_F, i.e., the resonant level, in both phases.

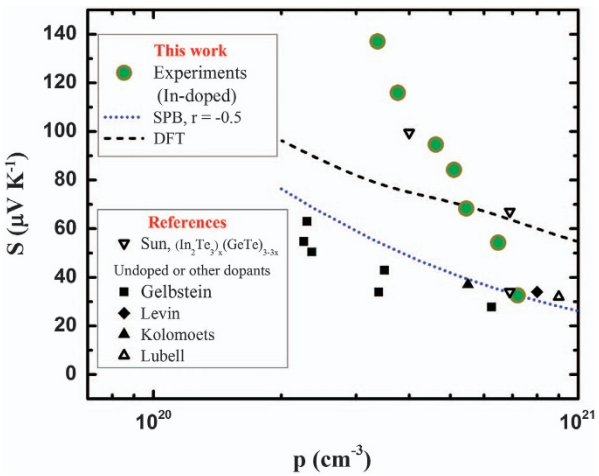

Figure 2 The room temperature Seebeck coefficient S as a function of the carrier concentration p (the Pisarenko relation). The experimental results of In-doped GeTe and theoretical calculations by the SPB model and density functional theory (DFT) are from the work presented here. Experimental results from the references are shown for comparison, including In_2Te_3-GeTe solid solution reported by Sun[58] and undoped GeTe or GeTe with other dopants reported by Levin,[34,60] Kolomoets,[61] and Lubell,[62] and Gelbstein.[63,64]

Compared with the undoped GeTe, the In-doped GeTe shows very similar resonant levels to those in the rhombohedral phase. The energy differences between the VBM and resonant levels are relatively small in both phases. The enhanced total DOS in both phases originates from the interaction between hosts and dopants, which do not depend on the actual crystal structure or temperature. Because the DDSs are around the Fermi levels, the DOS changes should contribute to a sizeable Seebeck enhancement.

Figures 1c and d show the calculated DOS for Ga-doped and Tl-doped GeTe in the rhombohedral phases. Similar to In, Ga can form a resonant level around the VBM, which changes the total DOS accordingly. The additional energy level leads to a narrow plateau near the VBM in $GaGe_{63}Te_{64}$. The difference between Ga- and In-doped GeTe is that the DOS peak in the former is hybridized with the VBM, which is probably due to the different energy level of its valent p states with respect to the VBM of GeTe. By contrast, Tl has almost no effect on the total DOS near the VBM. This non-monotonic trend from Ga, In to Tl has also been observed in PbTe, which is attributed to the relativistic effects in Tl.[57] Thus, compared with other group IIIA elements, indium contributes a much more distinct resonant level to the electronic bands of GeTe, which may lead to high thermoelectric response, according to our *ab initio* analysis. Thus, $In_xGe_{1-x}Te$ ($x = 0$, 0.01, 0.02, 0.03, 0.04, 0.05, and 0.06) compounds were synthesized to experimentally determine the influence of the resonant levels on

thermoelectric properties. The phase purity and compositions were analyzed by XRD and EDS (Supplementary Figures S1–S4). No obvious indium-containing impurity phases were found.

Figure 2 shows the Seebeck coefficient S as function of the carrier concentration p (the Pisarenko relation). The measured carrier concentrations of $In_xGe_{1-x}Te$ ($x=0$, 0.01, 0.02, 0.03, 0.04, 0.05, and 0.06) compounds are 7.2, 6.5, 5.5, 5.1, 4.6, 3.8, and 3.4×10^{20} cm^{-3}, respectively. The corresponding Seebeck coefficients are 33, 54, 68, 84, 95, 116, and 137 $\mu V\,K^{-1}$. A trend line (the dotted line) calculated by the single parabolic band (SPB) model is also obtained by considering a carrier effective mass of 1.28 m_e, with m_e as the free electron mass. An acoustic-phonon scattering is assumed (scattering parameter $r=-0.5$). The experimental Seebeck coefficients are much higher than the SPB results. We then calculate the Seebeck coefficient based on the real band structure of GeTe, as shown by the dashed line in Figure 2, and the theoretical Seebeck coefficients are not consistent with the high experimental ones in most $In_xGe_{1-x}Te$ compounds ($x>0.02$). Only the Seebeck coefficients of In_2Te_3-GeTe solid solution reported by Sun *et al.*[58] are consistent with the results herein, which indicates the uniqueness of the In dopants in the GeTe host.

The experimental data for undoped GeTe or GeTe with other dopants are collected for comparison.[34,59–64] The Seebeck coefficients in In-doped GeTe are considerably higher than those of samples with no dopant or with other dopants. For instance, the carrier concentration of $In_{0.06}Ge_{0.94}Te$ is similar to those of $Pb_{0.05}Ge_{0.95}Te$ and $(GeTe)_{0.97}(BiTe)_{0.03}$.[63,64] However, the Seebeck coefficient of $In_{0.06}Ge_{0.94}Te$ is three times as high as those of the Pb- or Bi-doped samples. Similarly, the Seebeck coefficient of $In_{0.01}Ge_{0.99}Te$ is twice the S value of an undoped GeTe,[63] which has a comparable carrier concentration of 6.3×10^{20} cm^{-3}. Considering the sizable difference in Seebeck coefficients between indium and other dopants, the resonant levels in In-doped GeTe should be responsible for the enhancement of the Seebeck coefficient. The greater Seebeck coefficient enhancements observed for samples with lower carrier concentrations can be rationalized by considering that the Fermi levels move closer to the resonant levels, which are above the VBM of the GeTe host.

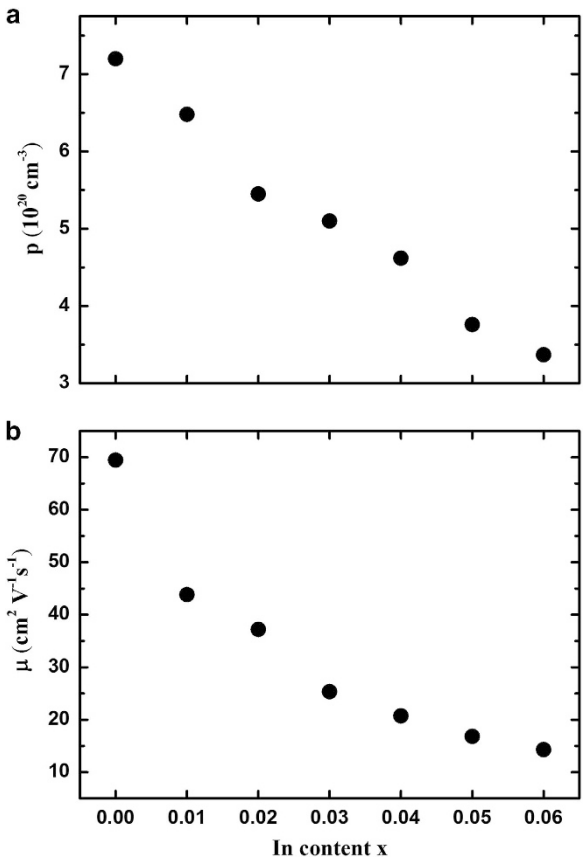

Figure 3 The indium content x-dependent room temperature (**a**) carrier concentration p and (**b**) carrier mobility μ in $In_xGe_{1-x}Te$ ($x=0$, 0.01, 0.02, 0.03, 0.04, 0.05, and 0.06) compounds.

Figure 3 shows the indium content x-dependent carrier concentration p and carrier mobility μ in $In_xGe_{1-x}Te$ ($x=0$, 0.01, 0.02, 0.03, 0.04, 0.05, and 0.06) compounds. The decrease in the hole concentration as the In content increases indicates that the In dopants may fill the germanium vacancies,

$$x\mathrm{In}_{\mathrm{In}}^{\times}+y\left(V_{\mathrm{Ge}}''+2h^{\cdot}\right)\rightarrow x\mathrm{In}_{\mathrm{Ge}}'+(y-x)V_{\mathrm{Ge}}''+(2y-x)h^{\cdot}. \qquad (2)$$

In most conventional thermoelectric materials, the carrier mobility increases as the carrier concentration decreases. However, the carrier mobility values μ in $In_xGe_{1-x}Te$ compounds have an opposite dependence on the carrier concentration, and they reduce significantly as the In content x increases. For instance, when the In content changes from $x=0$ to $x=0.06$, the carrier concentration and mobility reduce by ~53% and 80%, respectively. Moreover, the mobility reduction phenomenon is commonly observed in materials with resonant dopants.[45] The reduction in the carrier mobility should be mainly due to the increased density of ionized impurities as the dopant content becomes higher.

Figure 4 shows the temperature dependence of the Seebeck coefficient S, electrical resistivity ρ, and power factor ($PF=S^2/\rho$) for all $In_xGe_{1-x}Te$ ($x=0$, 0.01, 0.02, 0.03, 0.04, 0.05, and 0.06) compounds. The room temperature Seebeck coefficients in indium-doped samples are enhanced by a factor of between ~1.6 to 4.2, compared with that of the undoped GeTe. The advantages of a high Seebeck coefficient obtained by indium doping can be maintained across the measured temperatures. In the high-T cubic phases, the enhancement gradually reduces with increasing T, and the S values become close to that of the pristine sample at ~460 °C. However, In-doping severely increases the electrical resistivity, as both the carrier concentration and mobility become much smaller than those of the pristine sample.

Fundamentally, the transport characteristics of GeTe exhibit two stages, that is, a stage below and above the phase transition point. In addition, the transition point decreases as the dopant concentration increases. When the carrier concentration is high enough (for example, 7.2×10^{20} cm^{-3} for the undoped GeTe), the Seebeck coefficient S and resistivity ρ in both the rhombohedral and the cubic phase continue increasing as the temperature increases. The slopes of the S-T or ρ-T curves have two stages due to the phase transition. The curves are sharper in the low-temperature rhombohedral phase.[34] As shown in Figure 4, the undoped sample clearly displays such two-stage transport properties. S and ρ in the rhombohedral phase (below ~370 °C) both behave similar to those of degenerate semiconductors. The S-T and ρ-T slopes clearly decrease in the high-T phase. However, as the carrier concentration decreases, the S-T or ρ-T curves can exhibit different evolutions in the two phases. One difference is that the rhombohedral phase may experience both extrinsic and intrinsic transport,[64] as shown in the $x=0.05$ and $x=0.06$ doped samples. Below the phase transition point (which is already shifted to ~300 °C), the resistivity first increases, but then it decreases as the temperature increases, which indicates the intrinsic

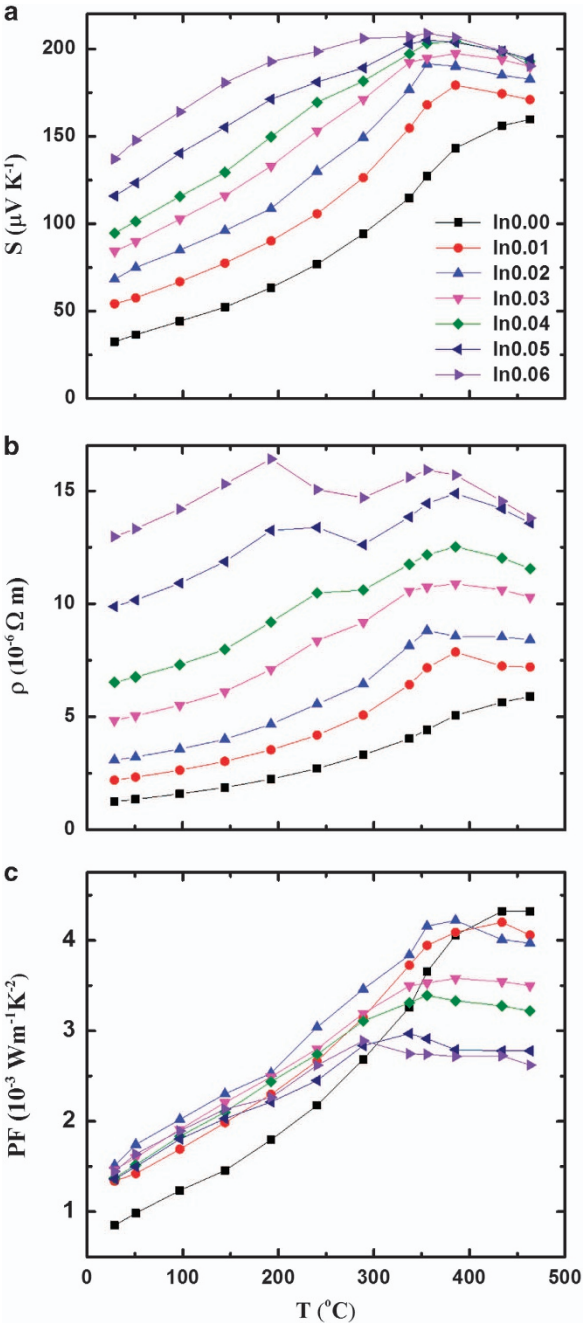

Figure 4 Temperature dependence of the (**a**) Seebeck coefficient S, (**b**) electrical resistivity ρ, and (**c**) power factor PF for $In_xGe_{1-x}Te$ ($x=0$, 0.01, 0.02, 0.03, 0.04, 0.05, and 0.06) compounds.

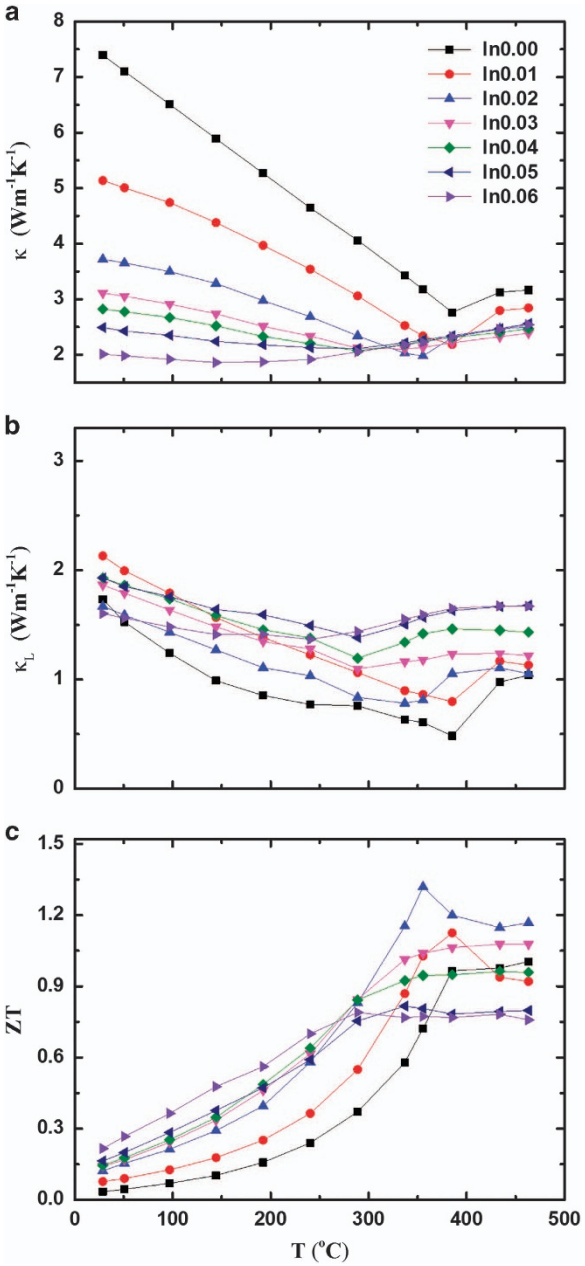

Figure 5 Temperature dependence of the (**a**) total thermal conductivity κ, (**b**) lattice thermal conductivity κ_L, and (**c**) figure of merit ZT for $In_xGe_{1-x}Te$ ($x=0$, 0.01, 0.02, 0.03, 0.04, 0.05, and 0.06) compounds.

conduction behavior. Correspondingly, the Seebeck coefficient curves gradually become flat as the temperature approaches the transition point. The other difference is that the slopes of the S-T and ρ-T curves become negative in the high-T cubic phase in the In-doped samples, which is possibly due to the thermal activation of electrons. The mixed conduction may start to influence the transport properties in the cubic phase. The Seebeck coefficient and resistivity then gradually reduce as the temperature increases.

Due to the trade-off between the enhanced Seebeck coefficient S and electrical resistivity ρ, the PF undergoes an increase in the lower temperature range but a decrease in the higher temperature range. The largest PF of $1.5\times10^{-3}\,W\,m^{-1}\,K^{-2}$ at room temperature appears in the $x=0.02$ sample, which is ~80% higher than that of the pristine GeTe. The maximum PF in the $x=0.02$ sample is $4.2\times10^{-3}\,W\,m^{-1}\,K^{-2}$ at 385 °C, which is close to the largest value obtained for the cubic phase undoped GeTe. Above 400 °C, the PF values in the indium-doped samples reduce, which is possibly due to the mixed conduction, as the enhancement of the Seebeck coefficient cannot compensate for the loss in resistivity.

Figure 5a shows the total thermal conductivity of $In_xGe_{1-x}Te$ ($x=0$, 0.01, 0.02, 0.03, 0.04, 0.05, and 0.06) compounds. κ is monotonically reduced by In-doping. The undoped GeTe has a large κ mainly because of its high carrier concentration and thus low electrical resistivity. Near the ferroelectric phase transition, the thermal

conductivity reaches its lowest point. Upon In doping, the κ-T slopes are lowered in the rhombohedral phase, and the κ-T curves become almost flat at high indium contents. The total thermal conductivity κ in thermoelectric materials generally can be divided into two components, electronic and lattice thermal conductivity, if the bipolar thermal conductivity is neglected.[65] Thus, we have the fundamental relation, $\kappa = \kappa_e + \kappa_L$, where κ_e and κ_L are the electronic and lattice thermal conductivity, respectively. The Wiedemann-Franz law $\kappa_e = LT/\rho$ directly connects the carrier contributions to the electrical and heat conduction, where L is the Lorenz number. L is dependent on the carrier concentration or Fermi level in the SPB model. The Lorenz numbers for $In_xGe_{1-x}Te$ compounds were calculated for each temperature point using the previously discussed theoretical method.[66] The Lorenz numbers decrease as the temperature or indium content increases, as shown in Supplementary Figure S5. Using these Lorenz numbers, the lattice thermal conductivity κ_L can be separated from the total thermal conductivity κ. As shown in Figure 5b, the lattice thermal conductivity κ_L of the doped samples becomes larger than that of the pristine GeTe above room temperature. The In-doped samples suffer from significantly reduced carrier concentrations and thus enhanced bipolar effects. Both the Seebeck coefficient and resistivity curves at high temperatures exhibit the mixed electron-hole conduction behavior. Therefore, the κ_L here should also include the bipolar term,[65] which potentially makes the calculated values of the doped samples larger.

Figure 5c shows the figure of merit ZT for all $In_xGe_{1-x}Te$ ($x = 0$, 0.01, 0.02, 0.03, 0.04, 0.05, and 0.06) compounds. The undoped sample shows ZT values of 0.03 and 1.0 at room temperature and 460 °C, respectively. The highest ZT can be improved to ~1.3 in the $In_{0.02}Ge_{0.98}Te$ compound at 355 °C. The best room temperature ZT is 0.2 in the $In_{0.06}Ge_{0.94}Te$ compound. The electrical terms (S^2p) and scattering terms (μ/κ) are calculated to determine the main contribution. At room temperature, the electrical terms are 0.76, 1.9, 2.5, 3.6, 4.1, 5.0 and $6.3 \times 10^{24}\,V^2\,K^{-2}\,m^{-3}$ for $x = 0$ to $x = 0.06$ samples, while the respective scattering terms are 9.4, 8.5, 10.0, 8.1, 7.3, 6.8 and $7.1 \times 10^{-4}\,S^2\,mK\,V^{-1}\,kg^{-1}$. The mobility loss has been compensated by the reduction in thermal conductivity, which results in similar scattering terms. Apparently, the enhanced ZT in indium-doped GeTe originates from the optimization of the electrical terms, due to the high thermoelectric response induced by the resonant levels. The average ZT is also important for thermoelectric applications in power generation and solid-state cooling, which is expressed as the integral of ZT over the working temperature range. The average ZT of the $In_{0.02}Ge_{0.98}Te$ compound is ~0.7 over the entire measured temperature range, which represents an ~70% enhancement on that of the undoped GeTe.

CONCLUSIONS

The indium dopants create resonant levels in both the rhombohedral and cubic phase GeTe, which contribute to a significantly enhanced thermoelectric response. Though the electrical resistivity is increased due to the reduced carrier concentration and mobility, the Seebeck enhancement compensates for such a loss in performance and leads to a higher power factor in most of the temperature ranges. The total thermal conductivity is remarkably reduced, which is primarily due to the decreased electronic contribution. Due to the Seebeck enhancement and thermal conductivity reduction, the figure of merit ZT has been improved to ~1.3 in the $In_{0.02}Ge_{0.98}Te$ compound. The corresponding average ZT is enhanced by ~70% over the entire temperature range. By screening other group IIIA dopants, we observe that resonant levels closer to the VBM are formed in Ga-doped GeTe, while no resonant level is found in Tl-doped GeTe. The strong resonant levels in In-doped GeTe may make it a promising base material in the search for an even higher thermoelectric performance.

CONFLICT OF INTEREST

The authors declare no conflict of interest.

ACKNOWLEDGEMENTS

We acknowledge support by the Natural Science Foundation of China under Grant Nos 11234012, 51572167, 51632005, 11604200 and 11674211. WZ acknowledges support by the Program of Shanghai Subject Chief Scientist (No 16XD1401100) and National Basic Research Program (973-program) of China under Project No. 2013CB632501. This work was also sponsored by the Natural Science Foundation of Shanghai (NO. 16ZR1448000) and The Program for Professor of Special Appointment (Eastern Scholar) at Shanghai Institutions of Higher Learning (No TP2015041). SW and JY acknowledge the financial support by the National Science Foundation under award number 1235535 and by the Inamori Foundation.

Author contributions: LW and XL contributed equally to this work. LW and SW synthesized the samples and performed the measurements of the TE properties. XL and Jiong Yang carried out first-principles calculations. TZ conducted the Hall effect measurements. LW, Jiong Yang, WZ, LC and Jihui Yang conceived the calculations/experiments and analyzed the results. LW, XL, Jiong Yang, WZ, and Jihui Yang wrote the manuscript, and all authors participated in editing.

1 Dresselhaus, M. S., Chen, G., Tang, M. Y., Yang, R. G., Lee, H., Wang, D. Z., Ren, Z. F., Fleurial, J. P. & Gogna, P. New directions for low-dimensional thermoelectric materials. *Adv. Mater.* **19**, 1043–1053 (2007).
2 Heremans, J. P., Wiendlocha, B. & Chamoire, A. M. Resonant levels in bulk thermoelectric semiconductors. *Energy Environ. Sci.* **5**, 5510–5530 (2012).
3 Yang, J., Yip, H.-L. & Jen, A. K.-Y. Rational design of advanced thermoelectric materials. *Adv. Energy Mater.* **3**, 549–565 (2013).
4 Slack, G. A. The thermal conductivity of nonmetallic crystals. *Solid State Phys* **34**, 1–71 (1979).
5 Morelli, D., Jovovic, V. & Heremans, J. Intrinsically minimal thermal conductivity in cubic I-V-VI_2 semiconductors. *Phys. Rev. Lett.* **101**, 035901 (2008).
6 Nielsen, M. D., Ozolins, V. & Heremans, J. P. Lone pair electrons minimize lattice thermal conductivity. *Energy Environ. Sci.* **6**, 570–578 (2013).
7 Zhang, Y., Skoug, E., Cain, J., Ozoliņš, V., Morelli, D. & Wolverton, C. First-principles description of anomalously low lattice thermal conductivity in thermoelectric Cu-Sb-Se ternary semiconductors. *Phys. Rev. B* **85**, 054306 (2012).
8 Zhao, L.-D., Lo, S.-H., Zhang, Y., Sun, H., Tan, G., Uher, C., Wolverton, C., Dravid, V. P. & Kanatzidis, M. G. Ultralow thermal conductivity and high thermoelectric figure of merit in SnSe crystals. *Nature* **508**, 373–377 (2014).
9 Sales, B., Mandrus, D. & Williams, R. K. Filled skutterudite antimonides: a new class of thermoelectric materials. *Science* **272**, 1325–1328 (1996).
10 Shi, X., Yang, J., Salvador, J. R., Chi, M., Cho, J. Y., Wang, H., Bai, S., Yang, J., Zhang, W. & Chen, L. Multiple-filled skutterudites: high thermoelectric figure of merit through separately optimizing electrical and thermal transports. *J. Am. Chem. Soc.* **133**, 7837–7846 (2011).
11 Takabatake, T., Suekuni, K., Nakayama, T. & Kaneshita, E. Phonon-glass electron-crystal thermoelectric clathrates: experiments and theory. *Rev. Mod. Phys.* **86**, 669 (2014).
12 Liu, H., Shi, X., Xu, F., Zhang, L., Zhang, W., Chen, L., Li, Q., Uher, C., Day, T. & Snyder, G. J. Copper ion liquid-like thermoelectrics. *Nat. Mater.* **11**, 422–425 (2012).
13 Qiu, W., Xi, L., Wei, P., Ke, X., Yang, J. & Zhang, W. Part-crystalline part-liquid state and rattling-like thermal damping in materials with chemical-bond hierarchy. *Proc. Natl. Acad. Sci. USA.* **111**, 15031–15035 (2014).
14 Qiu, W., Wu, L., Ke, X., Yang, J. & Zhang, W. Diverse lattice dynamics in ternary Cu-Sb-Se compounds. *Sci. Rep.* **5**, 13643 (2015).
15 Snyder, G. J., Christensen, M., Nishibori, E., Caillat, T. & Iversen, B. B. Disordered zinc in Zn_4Sb_3 with phonon-glass and electron-crystal thermoelectric properties. *Nat. Mater.* **3**, 458–463 (2004).
16 Hsu, K. F., Loo, S., Guo, F., Chen, W., Dyck, J. S., Uher, C., Hogan, T., Polychroniadis, E. & Kanatzidis, M. G. Cubic $AgPb_mSbTe_{2+m}$: bulk thermoelectric materials with high figure of merit. *Science* **303**, 818–821 (2004).
17 Poudel, B., Hao, Q., Ma, Y., Lan, Y. C., Minnich, A., Yu, B., Yan, X. A., Wang, D. Z., Muto, A., Vashaee, D., Chen, X. Y., Liu, J. M., Dresselhaus, M. S., Chen, G. & Ren, Z. F. High-thermoelectric performance of nanostructured bismuth antimony telluride bulk alloys. *Science* **320**, 634–638 (2008).

18 Biswas, K., He, J., Blum, I. D., Wu, C.-I., Hogan, T. P., Seidman, D. N., Dravid, V. P. & Kanatzidis, M. G. High-performance bulk thermoelectrics with all-scale hierarchical architectures. *Nature* **489**, 414–418 (2012).
19 Hu, L., Wu, H., Zhu, T., Fu, C., He, J., Ying, P. & Zhao, X. Tuning multiscale microstructures to enhance thermoelectric performance of n-type bismuth-telluride-based solid solutions. *Adv. Energy Mater.* **5**, 1500411 (2015).
20 Wang, S., Salvador, J. R., Yang, J., Wei, P., Duan, B. & Yang, J. High-performance n-type $Yb_xCo_4Sb_{12}$: from partially filled skutterudites towards composite thermoelectrics. *NPG Asia Mater.* **8**, e285 (2016).
21 Pei, Y., Shi, X., LaLonde, A., Wang, H., Chen, L. & Snyder, G. J. Convergence of electronic bands for high performance bulk thermoelectrics. *Nature* **473**, 66–69 (2011).
22 Liu, W., Tan, X., Yin, K., Liu, H., Tang, X., Shi, J., Zhang, Q. & Uher, C. Convergence of conduction bands as a means of enhancing thermoelectric performance of n-type $Mg_2Si_{1-x}Sn_x$ solid solutions. *Phys. Rev. Lett.* **108**, 166601 (2012).
23 Zhang, J., Liu, R., Cheng, N., Zhang, Y., Yang, J., Uher, C., Shi, X., Chen, L. & Zhang, W. High-performance pseudocubic thermoelectric materials from non-cubic chalcopyrite compounds. *Adv. Mater.* **26**, 3848 (2014).
24 Zhang, J., Song, L., Madsen, G. K. H., Fischer, K. F. F., Zhang, W., Shi, X. & Iversen, B. B. Designing high-performance layered thermoelectric materials through orbital engineering. *Nat. Commun.* **7**, 10892 (2016).
25 Zhao, L.-D., Tan, G., Hao, S., He, J., Pei, Y., Chi, H., Wang, H., Gong, S., Xu, H. & Dravid, V. P. Ultrahigh power factor and thermoelectric performance in hole-doped single-crystal SnSe. *Science* **351**, 141–144 (2015).
26 Pei, Y., Wang, H., Gibbs, Z. M., LaLonde, A. D. & Snyder, G. J. Thermopower enhancement in $Pb_{1-x}Mn_xTe$ alloys and its effect on thermoelectric efficiency. *NPG Asia Mater.* **4**, e28 (2012).
27 Parker, D., Chen, X. & Singh, D. J. High three-dimensional thermoelectric performance from low-dimensional bands. *Phys. Rev. Lett.* **110**, 146601 (2013).
28 Wu, L., Yang, J., Wang, S., Wei, P., Yang, J., Zhang, W. & Chen, L. Two-dimensional thermoelectrics with Rashba spin-split bands in bulk BiTeI. *Phys. Rev. B* **90**, 195210 (2014).
29 Wu, L., Yang, J., Wang, S., Wei, P., Yang, J., Zhang, W. & Chen, L. Thermopower enhancement in quantum wells with the Rashba effect. *Appl. Phys. Lett.* **105**, 202115 (2014).
30 Heremans, J. P., Jovovic, V., Toberer, E. S., Saramat, A., Kurosaki, K., Charoenphakdee, A., Yamanaka, S. & Snyder, G. J. Enhancement of thermoelectric efficiency in PbTe by distortion of the electronic density of states. *Science* **321**, 554–557 (2008).
31 Gelbstein, Y., Davidow, J., Leshem, E., Pinshow, O. & Moisa, S. Significant lattice thermal conductivity reduction following phase separation of the highly efficient $Ge_xPb_{1-x}Te$ thermoelectric alloys. *Phys. Status Solidi B* **251**, 1431–1437 (2014).
32 Chattopadhyay, T. & Boucherle, J. Neutron diffraction study on the structural phase transition in GeTe. *J. Phys. C: Solid State Phys.* **20**, 1431 (1987).
33 Damon, D., Lubell, M. & Mazelsky, R. Nature of the defects in germanium telluride. *J. Phys. Chem. Solids* **28**, 520–522 (1967).
34 Levin, E., Besser, M. & Hanus, R. Electronic and thermal transport in GeTe: a versatile base for thermoelectric materials. *J. Appl. Phys.* **114**, 083713 (2013).
35 Skrabek, E., Trimmer, D. in *CRC Handbook of Thermoelectrics* (ed Rowe D. M.) 267–275 (CRC Press, Boca Raton, FL, USA, 1995).
36 Chen, Y., Jaworski, C., Gao, Y., Wang, H., Zhu, T., Snyder, G., Heremans, J. & Zhao, X. Transport properties and valence band feature of high-performance $(GeTe)_{85}(AgSbTe_2)_{15}$ thermoelectric materials. *New J. Phys.* **16**, 013057 (2014).
37 Levin, E., Cook, B. A., Harringa, J., Bud'ko, S., Venkatasubramanian, R. & Schmidt-Rohr, K. Analysis of Ce- and Yb-Doped TAGS-85 materials with enhanced thermoelectric figure of merit. *Adv. Funct. Mater.* **21**, 441–447 (2011).
38 Levin, E., Bud'Ko, S. & Schmidt-Rohr, K. Enhancement of thermopower of TAGS-85 high-performance thermoelectric material by doping with the rare earth Dy. *Adv. Funct. Mater.* **22**, 2766–2774 (2012).
39 Gelbstein, Y., Davidow, J., Girard, S. N., Chung, D. Y. & Kanatzidis, M. Controlling metallurgical phase separation reactions of the $Ge_{0.87}Pb_{0.13}Te$ alloy for high thermoelectric performance. *Adv. Energy Mater.* **3**, 815–820 (2013).
40 Wu, D., Zhao, L.-D., Hao, S., Jiang, Q., Zheng, F., Doak, J. W., Wu, H., Chi, H., Gelbstein, Y. & Uher, C. Origin of the high performance in GeTe-based thermoelectric materials upon Bi_2Te_3 doping. *J. Am. Chem. Soc.* **136**, 11412–11419 (2014).
41 Perumal, S., Roychowdhury, S., Negi, D. S., Datta, R. & Biswas, K. High Thermoelectric performance and enhanced mechanical stability of p-type $Ge_{1-x}Sb_xTe$. *Chem. Mater.* **27**, 7171–7178 (2015).
42 Yang, J., Xi, L., Qiu, W., Wu, L., Shi, X., Chen, L., Yang, J., Zhang, W., Uher, C. & Singh, D. J. On the tuning of electrical and thermal transport in thermoelectrics: an integrated theory-experiment perspective. *npj Comput. Mater.* **2**, 15015 (2016).
43 Jaworski, C. M., Kulbachinskii, V. & Heremans, J. P. Resonant level formed by tin in Bi_2Te_3 and the enhancement of room-temperature thermoelectric power. *Phys. Rev. B* **80**, 233201 (2009).
44 Lan, J. L., Liu, Y. C., Zhan, B., Lin, Y. H., Zhang, B., Yuan, X., Zhang, W., Xu, W. & Nan, C. W. Enhanced thermoelectric properties of Pb-doped BiCuSeO Ceramics. *Adv. Mater.* **25**, 5086–5090 (2013).
45 Zhang, Q., Liao, B., Lan, Y., Lukas, K., Liu, W., Esfarjani, K., Opeil, C., Broido, D., Chen, G. & Ren, Z. High thermoelectric performance by resonant dopant indium in nanostructured SnTe. *Proc. Natl. Acad. Sci. USA* **110**, 13261–13266 (2013).
46 Mott, N. F. & Davis, E. A. *Electronic Processes in Non-Crystalline Materials* (Oxford University Press, Oxford, UK, 1971).
47 Liu, H., Yuan, X., Lu, P., Shi, X., Xu, F., He, Y., Tang, Y., Bai, S., Zhang, W. & Chen, L. Ultrahigh thermoelectric performance by electron and phonon critical scattering in $Cu_2Se_{1-x}I_x$. *Adv. Mater.* **25**, 6607–6612 (2013).
48 Sun, P., Wei, B., Zhang, J., Tomczak, J. M., Strydom, A., Søndergaard, M., Iversen, B. B. & Steglich, F. Large Seebeck effect by charge-mobility engineering. *Nat. Commun.* **6**, 7475 (2015).
49 Wang, S., Sun, Y., Yang, J., Duan, B., Wu, L., Zhang, W. & Yang, J. High thermoelectric performance in Te-free $(Bi, Sb)_2Se_3$ by structural transition induced band convergence and chemical bond softening. *Energy Environ. Sci.* **9**, 3436–3447 (2016).
50 Kresse, G. & Furthmüller, J. Efficient iterative schemes for *ab initio* total-energy calculations using a plane-wave basis set. *Phys. Rev. B* **54**, 11169 (1996).
51 Perdew, J. P., Burke, K. & Ernzerhof, M. Generalized gradient approximation made simple. *Phys. Rev. Lett.* **77**, 3865 (1996).
52 Kresse, G. & Joubert, D. From ultrasoft pseudopotentials to the projector augmented-wave method. *Phys. Rev. B* **59**, 1758 (1999).
53 Blöchl, P. E. Projector augmented-wave method. *Phys. Rev. B* **50**, 17953 (1994).
54 Yang, J., Li, H., Wu, T., Zhang, W., Chen, L. & Yang, J. Evaluation of half-heusler compounds as thermoelectric materials based on the calculated electrical transport properties. *Adv. Funct. Mater.* **18**, 2880–2888 (2008).
55 Madsen, G. K. & Singh, D. J. BoltzTraP. A code for calculating band-structure dependent quantities. *Comput. Phys. Commun.* **175**, 67–71 (2006).
56 Di Sante, D., Barone, P., Bertacco, R. & Picozzi, S. Electric Control of the Giant Rashba Effect in Bulk GeTe. *Adv. Mater.* **25**, 509–513 (2013).
57 Ahmad, S., Hoang, K. & Mahanti, S. *Ab initio* study of deep defect states in narrow band-gap semiconductors: group III impurities in PbTe. *Phys. Rev. Lett.* **96**, 056403 (2006).
58 Sun, H., Lu, X., Chi, H., Morelli, D. T. & Uher, C. Highly efficient $(In_2Te_3)_x(GeTe)_{3-3x}$ thermoelectric materials: a substitute for TAGS. *Phys. Chem. Chem. Phys.* **16**, 15570–15575 (2014).
59 Gelbstein, Y., Dado, B., Ben-Yehuda, O., Sadia, Y., Dashevsky, Z. & Dariel, M. P. Highly Efficient Ge-Rich $Ge_xPb_{1-x}Te$ thermoelectric alloys. *J. Electron. Mater.* **39**, 2049–2052 (2010).
60 Levin, E. Effects of Ge substitution in GeTe by Ag or Sb on the Seebeck coefficient and carrier concentration derived from Te 125 NMR. *Phys. Rev. B* **93**, 045209 (2016).
61 Kolomoets, N., Lev, E. Y. & Sysoeva, L. Nature of charge carriers in GeTe. *Sov. Phys. Solid State* **5**, 2101–2105 (1964).
62 Lubell, M. & Mazelsky, R. Carrier compensation in germanium telluride. *J. Electrochem. Soc.* **110**, 520–524 (1963).
63 Gelbstein, Y., Ben-Yehuda, O., Pinhas, E., Edrei, T., Sadia, Y., Dashevsky, Z. & Dariel, M. P. Thermoelectric properties of (Pb,Sn,Ge)Te-Based alloys. *J. Electron. Mater.* **38**, 1478–1482 (2009).
64 Hazan, E., Madar, N., Parag, M., Casian, V., Ben-Yehuda, O. & Gelbstein, Y. Effective electronic mechanisms for optimizing the thermoelectric properties of GeTe-rich alloys. *Adv. Electron. Mater.* **1**, 1500228 (2015).
65 Wang, S., Yang, J., Toll, T., Yang, J., Zhang, W. & Tang, X. Conductivity-limiting bipolar thermal conductivity in semiconductors. *Sci. Rep.* **5**, 10136 (2015).
66 Zhang, Y., Wu, L., Zhang, J., Xing, J. & Luo, J. Eutectic microstructures and thermoelectric properties of MnTe-rich precipitates hardened PbTe. *Acta Mater.* **111**, 202–209 (2016).

Supplementary Information accompanies the paper on the NPG Asia Materials website (http://www.nature.com/am)